MATERIALS SCIENCE

Large-area radiation-modulated thermoelectric fabrics for high-performance thermal management and electricity generation

Jin-Zhuo Liu[1,2,3]†, Wangkai Jiang[1,2]†, Sheng Zhuo[4,3], Yun Rong[1,3], Yuan-Yuan Li[1,3], Hang Lu[1,3], Jianchen Hu[1,2], Xiao-Qiao Wang[1,2], Weifan Chen[4], Liang-Sheng Liao[3]*, Ming-Peng Zhuo[1,2,3]*, Ke-Qin Zhang[1,2]*

Flexible thermoelectric systems capable of converting human body heat or solar heat into sustainable electricity are crucial for the development of self-powered wearable electronics. However, challenges persist in maintaining a stable temperature gradient and enabling scalable fabrication for their commercialization. Herein, we present a facile approach involving the screen printing of large-scale carbon nanotube (CNT)–based thermoelectric arrays on conventional textile. These arrays were integrated with the radiation-modulated thermoelectric fabrics of electrospun poly(vinylidene fluoride-co-hexafluoropropylene) (PVDF-HFP) membranes for the low-cost and high-performance wearable self-power application. Combined with the excellent photothermal properties of CNTs, the resulting thermoelectric fabric (0.2 square meters) achieves a substantial ΔT of 37 kelvin under a solar intensity of ~800 watt per square meter, yielding a peak power density of 0.20 milliwatt per square meter. This study offers a pragmatic pathway to simultaneously address thermal management and electricity generation in self-powered wearable applications by efficiently harvesting solar energy.

INTRODUCTION

Harvesting low-grade energy from the environment or human body toward affordable and sustainable electricity via piezoelectric (*1*), triboelectric (*2*), thermoelectric (*3*), and hydrovoltaic effect (*4*–*6*) have garnered substantial interest in self-power sensors (*7*), energy storage (*8*), and wearable electronics (*9*). Taking advantage of simple structure, desired mechanical flexibility, and direct heat-to-electricity conversion, the thermoelectric generators (TEGs) fibers were regarded as promising candidates for self-powered and wearable optoelectronics (*10*). Comprehensive thermal management of the heat collector, thermoelectric legs, and heat radiator offers an opportunity to optimize the output performance of the functional TEGs, as demonstrated in a previous attempt (*11*). To date, tremendous efforts have been adapted to modulate the intrinsic Seebeck coefficient and thermal/electronic conductivity of the thermoelectric materials for high-efficiency energy conversion (*12*). Nevertheless, these strategies generally suffer the high-temperature/pressure requirement or the sophisticated fabrication process, inducing a terrible hindrance to their practical applications (*13*). Impressively, the high TEG unit density and the obvious temperature gradient (ΔT) between TEGs hot and cool regions are also important for high-performance electricity generation (*14*, *15*).

To meet the evolving requirements of hot or cold comfort for smart textiles, the radiation-modulated strategies of solar photothermal and daytime radiative cooling demonstrated alternative opportunities (*16*). Silk functional fabric (*17*), metafabric (*18*), and white photothermal fabrics (*19*) introduce an innovative radiation regulation technique that uses sunlight to achieve thermal comfort for the human body. Furthermore, the passive daytime radiative cooling (PDRC) technique is proved to be a promising and sustainable technique for achieving outdoor cooling without additional energy supplements (*20*). Inspired by these successes (*13*, *21*), the radiation regulation technique could effectively increase the hot-region temperature of photothermal films or reduce the cool-region temperature of radiative cooling films to generate a desired ΔT for thermoelectric textile, which could simultaneously achieve the thermal comfort and the high electricity output (*22*, *23*). Typical schemes involve a wearable solar TEG with a maximum output voltage density of 23.4 V/m^2, which is dependent on the organic charge transfer cocrystal–based nanofiber membrane with a high photothermal conversion efficiency of 80.5% toward the desired ΔT (*24*). Notably, a high ΔT of 29.5 K was achieved in a flexible three-dimensional Janus helical ribbon architecture with the optimized photothermal heating and radiative cooling areas under a low solar radiation of 614 W/m^2 (*25*). However, the corresponding complex fabrication process presents a huge challenge to self-powered wearable applications (*26*). Furthermore, the sophisticated and efficient optoelectronic devices with desired device density were rationally constructed via a facile screen-printing method, benefiting from the low cost and large-area fabrication of wearable optoelectronics (*27*), which is rarely developed in textile field. Combing with the high ΔT induced by the integration of the photothermal heating and radiative cooling textiles (*28*), the screen printing provides a facile and scalable alternative for the accurate pattern definition and the high-resolution patterns creation of the high-performance thermoelectric arrays.

Herein, we purposefully selected the facile screen-printing technology to fabricate large-scale carbon nanotube (CNT)–based thermoelectric arrays with a device density more than 560 pairs on the commercial

[1]National Engineering Laboratory for Modern Silk, College of Textile and Clothing Engineering, Soochow University, Suzhou, Jiangsu 215123, China. [2]Jiangsu Provincial International Cooperation Joint Laboratory for Sustainable Textile Materials and Engineering in Universities, Suzhou 215021, China. [3]Institute of Functional Nano and Soft Materials (FUNSOM), Jiangsu Key Laboratory for Carbon-Based Functional Materials and Devices, Soochow University, Suzhou 215123, China. [4]School of Physics and Materials Science, Nanchang University, Nanchang 330031, China.
*Corresponding author. Email: lsliao@suda.edu.cn (L.-S.L.); Email: mpzhuo@suda.edu.cn (M.-P.Z.); kqzhang@suda.edu.cn (K.-Q.Z.)
†These authors contributed equally to this work.

fabric. In addition, a PDRC film displaying a reflectivity 96.9% and atmospheric transparent window emissivity 96.8% for excellent radiation cooling properties was prepared through the simple electrospinning mothed. The radiation-modulated thermoelectric fabric was constructed by sandwiched the PDRC film on the thermoelectric arrays. The spectral response difference between CNT intrinsic and the PDRC film was used to create a considerable ΔT for the thermoelectric array, enabling the preparation of a flexible wearable fabric with high light-to-heat conversion capability. After optimizing the cover area of PDRC film on the thermoelectric arrays, the functional fabric builds a high ΔT of 37 K under 0.8-sun natural sunlight, outputting a high voltage density of 6.67 V/m^2, which presents a potential application in the field of wearable electronic products. It offers a lightweight and cost-effective approach to collecting solar energy, enabling the mass production of flexible electronic devices and facilitating practical applications.

RESULTS

Design and manufacture of radiation-modulated thermoelectric fabric

Solar irradiance absorption and reflection not only are necessary to achieve the thermal comfort for hummus via photothermal and radiative cooling effects (*29*) but also could be harnessed to generate a temperature gradient for the wearable thermoelectrical devices (*30*). Poly(vinylidene fluoride) (PVDF) derivates of the poly(vinylidene fluoride-co-hexafluoropropylene) (PVDF-HFP) holds the high stretchability and mechanical stability, which are promising candidates for the optoelectronic and smart fibers application (*31*). It is well known that the electrospinning technology demonstrates the flexibility, facile, low cost, and mass production for the fabrication of nanofiber membranes (*32*). The PVDF-HFP was rationally chosen to construct the large-scale nanofiber membrane via the electrospinning technology (fig. S1A) for the radiative cooling application (Fig. 1A). As shown in the scanning electron microscopy (Fig. 1B and fig. S1, B and C), the as-prepared PVDF-HFP nanofibers show a smooth surface and a relatively uniform diameter across 0.3 to 1.6 μm with average diameter of ~0.8 μm, suggesting the successful preparation of the PVDF-HFP nanofiber membrane. An additional characteristic that renders PVDF-HFP particularly suitable for radiative cooling is its minimal absorption loss across the entire solar spectrum, coupled with a refractive index of approximately 1.42 (fig. S2). According to the Mie scattering theory (*33*), the fiber diameter distribution close to the waveband of the solar spectrum is favorable to achieving the high solar scattering efficiency for radiative cooling applications. The finite elements analysis (FEA) method was used to calculate the scatter efficiency of these prepared PVDF-HFP nanofiber membrane with fiber diameter across 0.3 to 1.6 μm, which demonstrates strongly scattered sunlight covering most of the solar wavelength range (Fig. 1C). This theoretical calculation is consistent with the bright white visual appearance of PVDF-HFP nanofiber films as shown in fig. S1D. As presented in Fig. 1D, the PVDF-HFP nanofiber films display an obvious spectrum selective property with a high reflectivity of more than 96.9% with thickness of 550 μm (fig. S3) in the sunlight region (0.3 ~2.5 μm) and a high emissivity of 96.8% in the middle infrared range, which is beneficial for daytime radiative cooling (*34*). Notably, these prepared PVDF-HFP nanofiber membranes slowly heated up from 26.8° to 43.8°C by open environment measurements after being irradiated by a 1-sun air mass (AM) 1.5 simulator for 1500 s. Then, the final equilibrium temperature displays 9.6°C lower than that of substrate white fabric. On the contrary, the photothermal layer quickly heated up from 27.1° to 80.8°C, and the final equilibrium temperature displays 27.4°C higher than that of the substrate white fabric. Besides, 10 cycles of heating cycle stability tests were conducted on the white-cloth layer and radiative cooling layer (fig. S4), which confirms that the radiative cooling layer has a stable and low temperature compared with the white cloth. In summary, radiative cooling layer and photothermal layers could create a great temperature gradient of 37°C under solar irradiation (Fig. 1E). Therefore, combining photothermal and radiative cooling effect facilitates higher temperature gradients.

Photothermal performance of screen printing–based photo-thermoelectric array

Impressively, the screen-printing process (fig. S5) was regarded as the promising approach for the scalable production of thermoelectric arrays on fabric due to its high pattern flexibility, high productivity, and cost-effective production capability (*35*). It is well known that the high viscosity of the ink is necessary to prepare nanoscale films with two-dimensional structure via screen-printing process, creating the unlimited access to substrates and patterns (*36*). Compared with traditional inorganic thermoelectric materials, the CNT has a multitude of beneficial characteristics, including low toxicity, chemical stability, outstanding electrical conductivity, exceptional mechanical strength, photothermal properties, and high Seebeck coefficient, which make it the ideal material for the thermoelectric array (*37*, *38*). The rheological properties of the CNT-based ink confirmed that its relatively high viscosity is cohesive and sticky, improving the printing quality (fig. S6), which is favorable for the scalable production of thermoelectric arrays via screen-printing method. However, the excess high viscosity is also terrible for the screen-printing process (fig. S7). The copious interstices and voids of micro- and nano-dimensions amid the fibers engendered a potent capillary force, compelling the CNT to adhere uniformly and tenaciously onto the surface of the fabric (fig. S8). Typically, the CNT-based thermoelectric arrays with a high assembly density of thermoelectric array (TEG unit: 560 pairs) and their linked silver arrays were successfully prepared on a large fabric with size of 1 m by 0.2 m via screen-printing method as verified in Fig. 2 (A and B). Furthermore, a logo of "Soochow University" based on the CNT was also screen-printed on commercial white fabric to illustrate the high pattern flexibility of screen-printing process (Fig. 2C), suggesting the desired proposed design. The infrared images revealed that the Soochow University logo printed on the fabric gradually became brighter and distinct after simulated sunlight for 10 and 20 s. It powerfully clarified the excellent photothermal property of these screen-printed CNT patterns, which demonstrates to be highly advantageous for infrared thermal imaging applications. Moreover, the temperature increments of the CNT exhibit a typical solar illumination intensity-dependent photothermal characteristic upon exposure to simulated sunlight irradiation at the different simulated sunlight intensities (Fig. 2D). The maximum temperatures rise to 44.8°, 53.6°, 61.9°, and 70.1°C simulated by the sunlight with 0.25-, 0.5-, 0.75-, and 1-sun intensity, respectively. As shown in Fig. 2E, temperature variations are proportional to the different simulated solar illumination intensities in heating and cooling processes during 0 to 720 s. As depicted in fig. S9, the observed linear relationship between ΔT and power densities indicates that the temperature could be controlled by adjusting excitation power. The maximum temperature is in keeping with Fig. 2E,

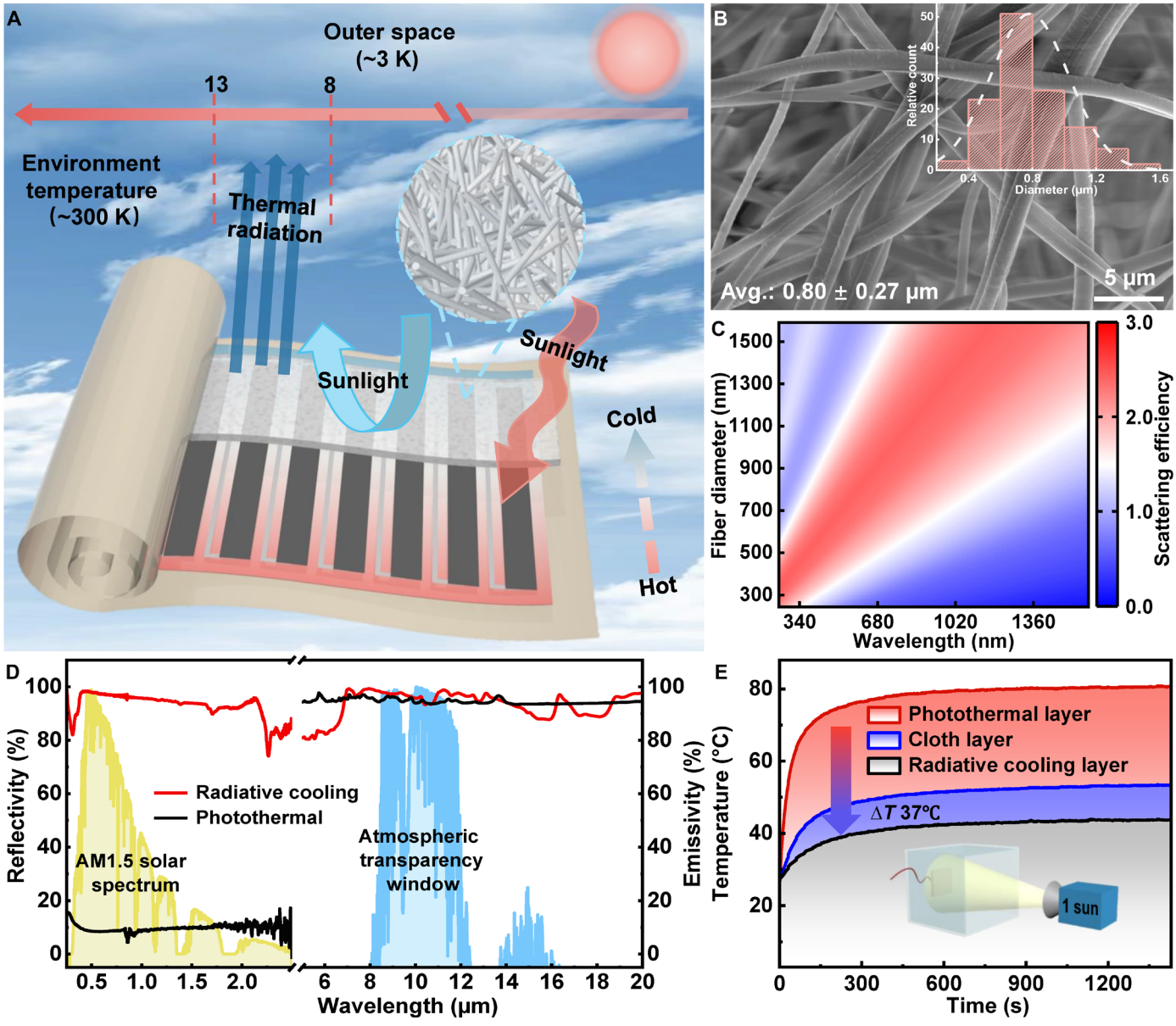

Fig. 1. Design and manufacture of radiation-modulated thermoelectric fabric. (**A**) Principle and the structures of wearable thermoelectrical device. (**B**) The representative scanning electron microscopy images of PVDF-HFP membrane. The insert was the diameter distribution of PVDF-HFP fiber in the membrane. (**C**) Scattering efficiency of circular vacancy in PVDF-HFP membrane. (**D**) Reflectivity and emissivity spectra of radiative cooling and photothermal. (**E**) Temperatures of photothermal layer, cloth layer, and radiative cooling layer after a period of irradiation with 1-sun intensity (ambient temperature, 25°C). S, seconds.

which illustrates the outstanding solar illumination intensity dependence and photostability of CNT. After undergoing 10 cycling tests of heating and cooling process, the prepared CNT pattern also maintains the maximum temperature of ~70°C, suggesting high photothermal stability (Fig. 2F). These results demonstrate that the CNT-based pattern prepared by screen-printing method exhibits excellent photothermal conversion efficiency and pattern resolution, which is sufficient to meet the needs of making high-precision thermoelectric arrays.

Thermoelectric performance of thermoelectric array

A thermoelectric array composed of 28 thermoelectric pairs was fabricated on a 10 cm–by–10 cm commercial white fabric as depicted in Fig. 3 (A_1). The black pattern corresponds to the CNT thermoelectric arrays printed three times, with a width of ~3.5 mm and a thickness of ~57 μm (Fig. 3, A_2, and fig. S10). A laboratory-made thermoelectric testing system (fig. S11 and note S1) was developed to confirm the thermoelectric performance of thermoelectric arrays. The CNT line patterns exhibiting high p-type Seebeck coefficients were subsequently connected in series by silver electrodes with a line width of 0.5 mm form integrated TEG device. Notably, a thermoelectric array comprising 14 thermoelectric pairs demonstrates an obvious enhancement in the output voltage from 0.58 to 4.63 mV while increasing the ΔT from 1 to 8 K (Fig. 3B), suggesting a remarkable total Seebeck coefficient of 1.16 mV/K. Furthermore, it is clearly found that the total Seebeck coefficient is proportional to the number of

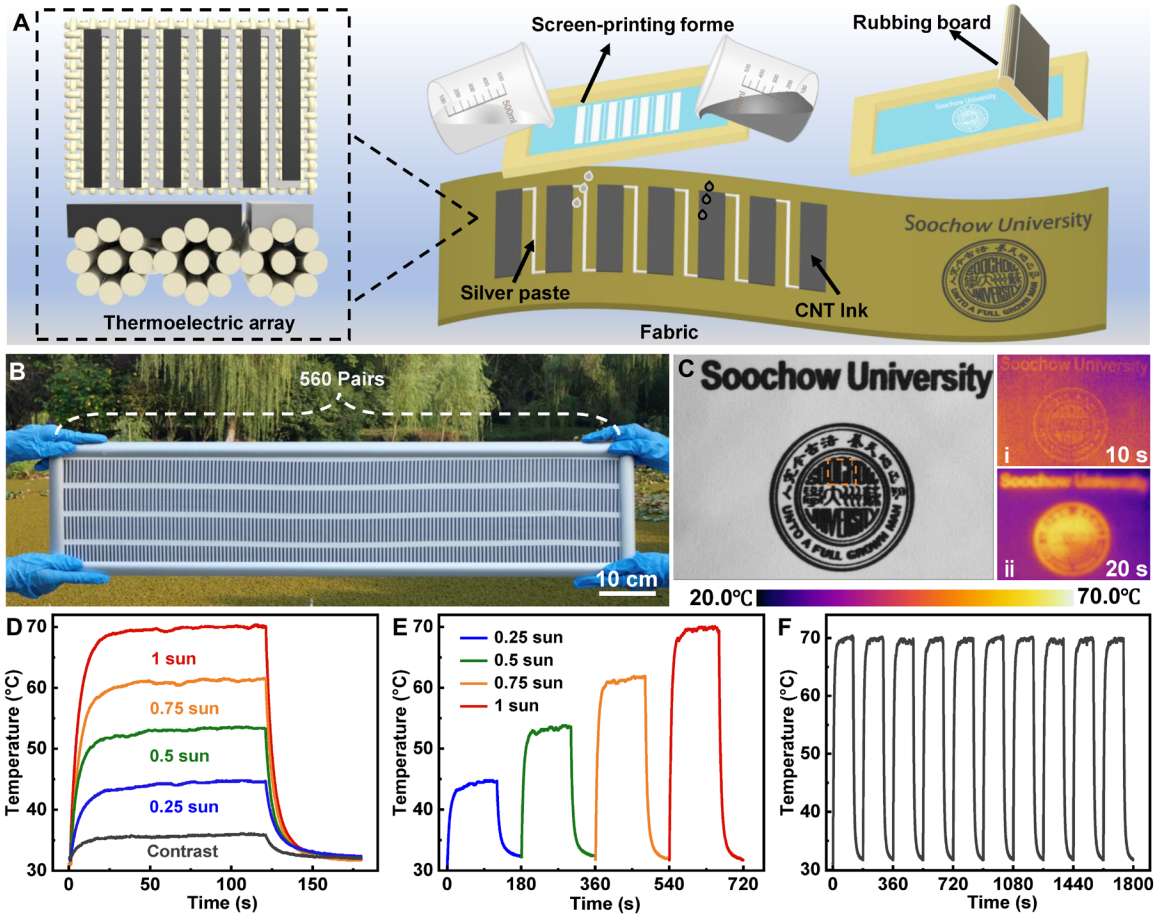

Fig. 2. Photothermal performance of screen-printing based photo-thermoelectric array. (**A**) A schematic showing the screen-printing process. (**B**) Large-area fabric printed with thermoelectric arrays. (**C**) Image of Soochow University logo printed on fabric and infrared images of Soochow University logo corresponding to different illumination times, respectively. (**D** and **E**) Temperature variations of CNT at 0.25 (blue line), 0.5 (green line), 0.75 (orange line), and 1 sun (red line). (**F**) Ten heating and cooling cyclic tests of CNT at 1 sun. S, seconds.

thermoelectric arrays. As presented in Fig. 3C reveals, the CNT and silver components exhibit a p-type Seebeck coefficient of 50 μV/K and n-type Seebeck coefficient of −5 μV/K, respectively. Moreover, the electrical conductivity of the CNT and silver paste are 700 and 7 ohm/m, respectively, indicating a satisfactory compatibility and performance match. As shown in Fig. 3D, the power density and circuit current of the thermoelectric array vary with the voltage output at different ΔT. The voltage output of the thermoelectric array achieves a maximum of 5.8 mV after increasing ΔT to 9 K. In addition, the short-circuit current decreases linearly with the output voltage, achieving a value of approximately 0.8 μA at $\Delta T = 9$ K. Furthermore, the thermoelectric array exhibits a maximum power density of 1.04 W/m^2 at $\Delta T = 9$ K, undergoing an external resistance of 5.6 kilohm (Fig. 3E). The consideration of washing resistance of the fiber-based optoelectronic is imperative for the practical application of the flexible wearable fabrics. To simulate real washing processes, the thermoelectric array fabric was immersed in a beaker containing tap water at 25°C and subjected to rolling washing for 20 min per cycle as depicted in Fig. 3F. Following multiple washes in tap water, the resistance of the thermoelectric array experienced a slight increase from 1.0 to 1.3 kilohm after 10 cycles. The final resistance change (R/R_0) remained at approximately 1.3, where R was the resistance after thermoelectric array washing and R_0 was its initial resistance. Similarly, the Seebeck coefficient exhibited a relatively stable trend after 10 washing cycles, ultimately stabilizing at around 48 μV/K with a minor change of about 5% (Fig. 3G). All of these elucidate the exceptional washing resistance of the thermoelectric array fabric. When stored in an environment with temperatures ranging from 16° to 26°C and humidity levels between 30 and 50% for a duration of 12 months, the resistance and cooling performance of the thermoelectric textiles remain remarkably stable, demonstrating exceptional durability (fig. S12). Furthermore, to evaluate the durability of the fabric when subjected to sustained high strain, a series of more than 2000 bending-release cycles were performed at a strain level of 50% (fig. S13). The bending-releasing curve demonstrated consistent repeatability. Considering the complex working environment of the thermoelectric array fabric, it was necessary to evaluate the sensor's performance under bending and twisting conditions (*39*). The relative resistance changes were observed during these movements, as shown in Fig. 3H. Under tensile deformation exceeding 50%, the Seebeck coefficient remains at 49 μV K^{-1}, with a variation of less than 4% from its natural state, demonstrating the exceptional thermoelectric performance of thermoelectric array even under tensile deformation (fig. S14). The relative resistance increases with higher strain and returns to its initial value

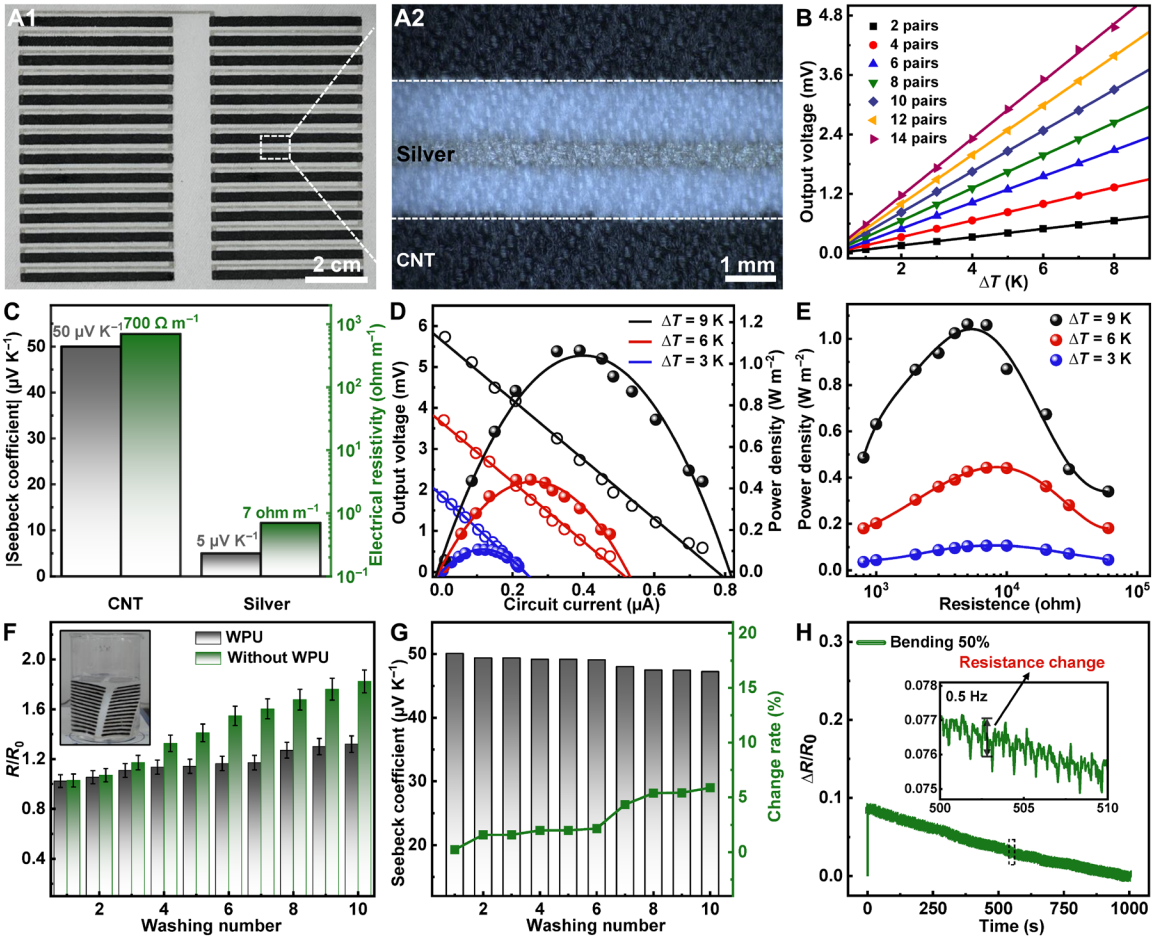

Fig. 3. Thermoelectric performance of thermoelectric array. (**A**) Twenty-eight pairs of thermoelectric arrays and optical electron microscopy magnification in the dotted box. (**B**) The variations of output voltage along with thermoelectric array pairs and Δ*T*. (**C**) The Seebeck coefficient and electrical resistivity of CNT and silver, respectively. (**D**) The output voltage and output power density as a function of circuit current when Δ*T* = 3, 6, and 9 K. (**E**) The output power density as a function of load resistance when Δ*T* = 3, 6, and 9 K. (**F**) The resistance changes of the thermoelectric arrays under cyclic washing. (**G**) The Seebeck coefficient changes of the thermoelectric arrays and change rate under cyclic washing. (**H**) The resistance changes of the thermoelectric arrays under cyclic bending. S, seconds.

upon release, which illustrates the desired exceptional sensing performance of the thermoelectric array fabric in bending and twisting scenarios for practical application.

Output performance of radiation-modulated thermoelectric fabric

The fundamental principle underlying thermoelectric power generation relies on the Seebeck effect, which leverages the temperature gradient between two surfaces of the device to facilitate the movement of charge carriers (*40*). To achieve higher output voltage and power, it is effective to enhance the performance of the thermoelectric array by increasing its area, assembly TEG unit density, or the applied Δ*T*. The PVDF-HFP nanofiber membranes with promising radiative cooling performance were deposited on the CNT-based thermoelectric array to create a cold region under solar irradiation to generate a considerable thermoelectric potential (Fig. 4A). The photo in Fig. 4B shows a radiation-modulated thermoelectric fabric with size of 10 cm by 10 cm, which consists of thermoelectric fabric with 28 pairs and PVDF-HFP nanofiber membranes with thickness of 0.55 mm. In details, the CNTs and PDRC films create alternate hot and cold regions under solar irradiation for an obvious Δ*T*, which facilitates charge carriers (holes) to diffuse in the CNTs from hot to cold regions, enabling the generation of thermoelectric potential. To assess the performance of radiation-modulated fabric, the FEA method was used to simulate the temperature difference across the thermoelectric array under solar irradiation of 0.5 sun at an ambient temperature of 25°C. As illustrated in Fig. 4C, the temperature of the hot side could achieve 55°C and engender a Δ*T* of 25 K when the temperature of the cold side maintains 30°C (note S2). It is powerfully confirmed that the radiation-modulated fabric could create obvious temperature gradient between hot regions and cold regions. An indoor-simulated solar test (Fig. 4D) was conducted to evaluate the Δ*T* between hot sides and cold sides of thermoelectric array. As shown in Fig. 4E and fig. S15, the maximum Δ*T* of the PDRC films with coverage ratio (x:y) of 0.5 rise to 15.7°, 24.2°, 31.9°, and 41.4°C with the simulated sunlight intensities of 0.25, 0.5, 0.75, and 1 sun, respectively. The temperature slope and output voltage were further improved by controlling the coverage ratio (x:y) of PDRC films (x) on thermoelectric array (y) under 0.25 sun. Previously, because of the existence of parasitic heat conduction, the different

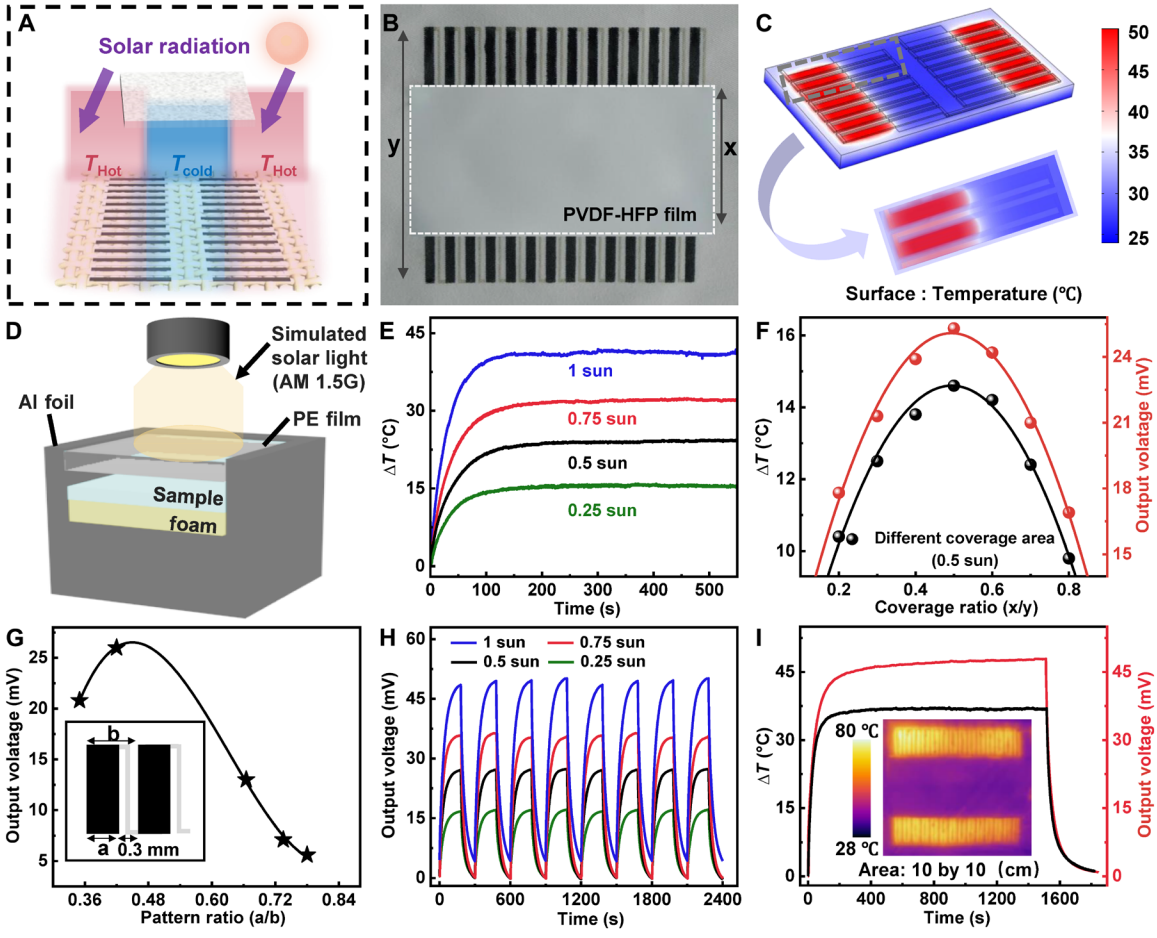

Fig. 4. Output performance of radiation-modulated thermoelectric fabric. (**A**) Cooling/heating components for daytime thermal gradients and thermoelectric array for thermoelectric generation. (**B**) The schematic diagram of the radiation-modulated fabric. (**C**) FEA result showing the temperature distribution across the thermoelectric array. (**D**) The schematic diagram of the installation for investigating the outdoor radiation-modulated fabric performance. (**E**) The temperature difference variations of radiation-modulated fabric under 0.25 (green line), 0.5 (black line), 0.75 (red line), and 1 sun (blue line)–simulated sunlight intension, respectively. (**F**) Temperature difference and output voltage of PDRC films with different coverage areas under 0.5 sun–simulated sunlight intensity. (**G**) Effect of thermoelectric array pattern ratio on output voltage and a schematic diagram coated with CNTs (inset). (**H**) Radiation-modulated fabric cyclic tests of the output voltage at 0.25, 0.5, 0.75, and 1 sun–simulated sunlight intensity. (**I**) Temperature difference and output voltage of radiation-modulated fabric under 1 sun–simulated sunlight intensity. S, seconds.

areas of the hot region and the cold region will affect the construction of the temperature gradient of the radiation-modulated thermoelectric fabric. As shown in Fig. 4F, the radiation-modulated fabric yielded a maximum ΔT of 14.5°C and V_{oc} of 16 mV at a coverage ratio of 0.5 due to reduction of the parasitic heat flow (conduction/convection). Besides the proportional system, the pattern size (fig. S16) could affect both the assembly TEG unit density of the thermoelectric array and the temperature gradient, thereby affecting the total thermoelectric potential. As depicted in Fig. 4G, the output voltage corresponding to pattern sizes of 0.35, 0.42, 0.665, 0.735, and 0.78 were 20.8, 26, 13, 7.1, and 5.6 mV, respectively. Thus, the pattern size (a:b) is also a key parameter to modulate the output voltage of thermoelectric array under the solar irradiation. The voltage of radiation-modulated fabric could reach 16.8, 27.1, 36.3, and 49.5 mV corresponding to the 0.25-, 0.5-, 0.75-, and 1 sun–simulated sunlight intensities as verified in Fig. 4H. Furthermore, eight light on/off cyclic tests were conducted under different simulated sunlight intensities, which demonstrate a constant maximum of output voltage and confirm the cycling stability of radiation-modulated fabrics (Fig. 4H). In particular, the optimal ΔT of the radiation-modulated thermoelectric fabrics with coverage ratio of 0.5 and pattern ratio of 0.42 could reach 37.1°C, and the output voltage reaches 47.9 mV and a power density of 0.32 mW/m^2 under 1 sun of simulated sunlight intensity (Fig. 4I and table S1). As a short conclusion, the designed radiation-modulated thermoelectric fabric demonstrated outstanding and stability of solar light collection for excellent energy conversion from heat to electricity.

The application of radiation-modulated thermoelectric fabric

Continuous temperature (fig. S17) and output voltage tracking outdoor experiments (Fig. 5, A and B) were implemented on 6 September (Suzhou: 31°18′6.1″N, 120°34′51.9″E, the real-time temperature, humidity, and wind velocity as shown in table S2), which demonstrates the photo-thermoelectric conversion performance of the radiation-modulated thermoelectric fabric upon natural sunlight. Specifically, the devices consist of an extruded polystyrene foam board that is enveloped in aluminum (Al) strips, designed to reflect sunlight and

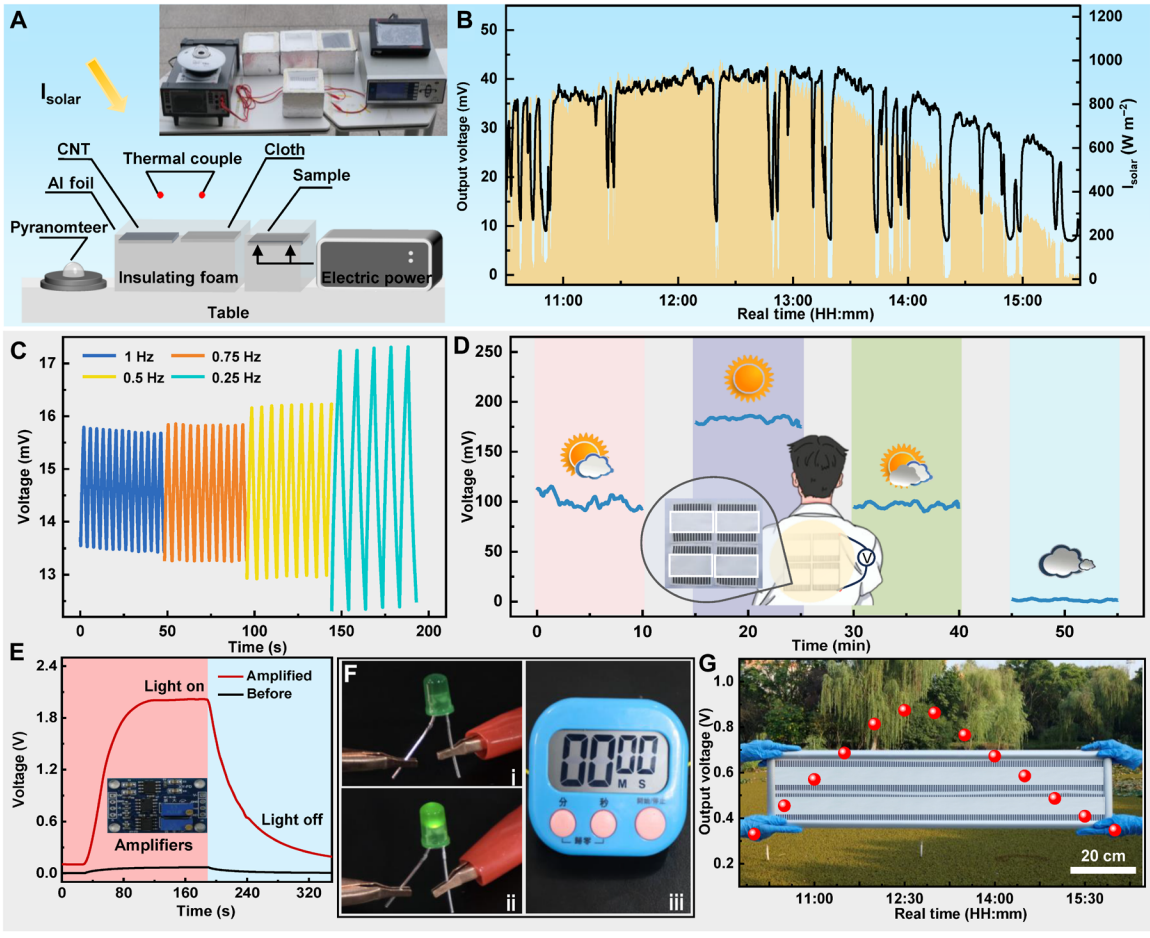

Fig. 5. The application of radiation-modulated thermoelectric fabric. (**A**) The schematic illustration of radiation-modulated thermoelectric fabric for the measurement of U_{oc}. (**B**) The real-time output voltage data of radiation-modulated fabric under natural light at Suzhou (China) on 6 September 2023. (**C**) The real-time output voltage data of radiation-modulated fabric under natural light at Soochow (China) on 6 September. (**D**) Output voltage generation performance of self-powered wearable textile under four different weather conditions. Inset, schematic diagram of applications in self-powered wearable textile. (**E**) Amplifying the voltage of wearable textile using amplifiers. (**F**) Demonstration of using amplified voltage to light up a green light-emitting diode and timer. (**G**) The real-time output voltage data of radiation-modulated fabric under natural light at Suzhou (China) on 7 September 2023. S, seconds. Min, minutes.

ambient radiation, along with a layer of highly transparent polyethylene film that serves as an effective barrier against convective heat transfer (fig. S18). The outdoor voltage test of the as-prepared radiation-modulated thermoelectric fabric was carried out under natural sunlight. The output voltage is consistent with variation of solar irradiance, which reaches the maximum output voltage of 42.7 mV at 12:30 as verified in Fig. 5B. As depicted in fig. S19A, the output voltage is consistent with variation of solar irradiance, which reaches the maximum output voltage of 40 mV at 12:30 with a temperature of 36°C in Suzhou (China) on 26 August 2024. Since the radiative cooling film can emit infrared radiation to dissipate heat, electricity is also generated at night, showing an output voltage of 0.5 mV in Suzhou (China) on 26 August 2024 (fig. S19B). Significantly, the outdoor experiments profoundly confirm the excellent radiative cooling performance of PDRC films and the effective photo-thermoelectric conversion of flexible CNT-based thermoelectric array. Radiation-modulated thermoelectric fabric with desired flexible and lightweight feature could perform excellent photo-thermoelectric power generation sustainably and stably, benefiting the wide application in wearable electronics. The variations in covering frequency of the swinging arm affect the blocking or transmission of radiation through the fabric, thus influencing the voltage output. By measuring the voltage output changes, it may be possible to gather valuable information about radiation exposure, which could help monitor and assess potential health risks. A homemade device (fig. S20) consisting of xenon lamp with AM 1.5 filter and liner motor was set up to confirm the sensing function of radiation-modulated thermoelectric fabric. Under simulated sunlight with 1-sun intensity, the maximum voltage at frequencies of 0.25, 0.5, 0.75 and 1 Hz are 15.7, 15.9, 16.2, 17.2 mV, which confirms the related relationship between the voltage amplitude and the swing arm frequency (Fig. 5C). Under different oscillation frequencies, the potential changes are identifiable, the voltage change rate accelerates, and the numerical change range gradually narrows as the oscillation frequency increases. Radiation-modulated thermoelectric fabric not only has motion sensing functions but also effectively collects sunlight and performs thermoelectric conversion. At the same time, it showed good air permeability comparable to that of denim fabric (fig. S21). Furthermore,

these PVDF-HFP membranes were seamlessly integrated with thermoelectric fabrics for enhanced durability and wearability through simple and traditional sewing techniques. When combined with the effective thermal barrier of practical garments, it is safe for the human body. Four pieces of radiation-modulated thermoelectric fabrics (inset of Fig. 5D) were assembled on clothing to explore its outdoor wearable photothermal conversion effect, and its outdoor output voltage was tested on a sunny day on 7 September, with an average temperature of 30°C. As the intensity of sunlight changes, the output voltage fluctuates accordingly. Typically, the output voltage could reach 115.2, 184.5, 100.6, and 2.9 mV at four different times on a clear day, respectively (Fig. 5D). Besides, radiation-modulated thermoelectric fabric could achieve the driving of small wearable devices with the help of amplifiers. The radiation-modulated thermoelectric fabric with 28 pairs thermoelectric array under 1 sun reach 0.06 and 2.0 V before or after amplification, respectively, which is enough to drive most electronic devices (Fig. 5E). Moreover, the radiation-modulated thermoelectric fabric was connected to a voltage booster circuit, where its practical application demonstrated when it powered on a green light-emitting diode and a timer by harvesting solar energy via a voltage amplifier, as illustrated in Fig. 5F and fig. S22. For demonstrating the scalable manufacturability of radiation-modulated thermoelectric fabric, the fabric with size of and 560 pairs of thermoelectric units was fabricated, highlighting its potential for industrial implementation. As shown in Fig. 5G, the output voltage of the prepared thermoelectric fabric with size of 1 m by 0.2 m under natural light was investigated from 10:00 to 16:00. The voltage density is consistent with the variation in solar irradiance, reaching a maximum of 6.67 V/m^2 and a peak power density of 0.20 mW/m^2 at 12:30, which is higher than the current standards (table S1). It is suggested that the current performance and area have considered advantages compared with the previous thermoelectric fibers, which is favorable for future self-powered wearable applications.

DISCUSSION

In conclusion, we successfully fabricated PVDF-HFP–based radiative cooling fiber membranes and CNT-based photothermal/thermoelectric arrays using electrostatic spinning and screen-printing technologies, respectively. By combining these elements and coating the PVDF-HFP–based fiber membrane with the CNT-based arrays, we designed scalable and flexible radiation-modulated thermoelectric fabrics. These fabrics achieve the desired thermal management and effectively harvest thermal energy for affordable and sustainable electricity generation. The controlled coverage ratio of the PVDF-HFP–based fiber membrane on the CNT-based arrays allows precise adjustment of the temperature gradient across the thermoelectric array, enhancing energy convention performance from thermal to electrical energy. Leveraging the distinct spectral properties of PVDF-HFP and CNT, we achieved an impressive temperature gradient of 37 K across the thermoelectric array under 1-sun solar irradiation. Notably, our fabrics demonstrated a high output voltage density of 6.67 V/m^2 under a solar density of 800 W/m^2 in outdoor solar thermoelectric conversion tests, showcasing promising potential for wearable solar energy harvesting. Moreover, these fabrics exhibit the capability to harness energy in outdoor environments, enable sensing functionalities, and power small-scale electronic devices. Therefore, our proposed radiation-modulated fabrics offer a promising avenue for effectively using low-grade heat from the surroundings to supply power for wearable electronics and various other applications.

MATERIALS AND METHODS

Materials

The materials used for this study are as follows: *N*,*N*-dimethylformamide (CSA, 68-12-2), acetone (CSA, 7-64-1), PVDF-HFP (CSA, 9011-17-0), waterborne polyurethane (CSA, 9999-99-9), and single-walled CNTs (SWCNTs) aqueous dispersion (batch number, 22102020).

Fabrication of PVDF-HFP nanofiber membranes

N, *N*-dimethylformamide (7.28 g) and acetone (3.12 g) were added into a glass bottle to prepare a mixed solution with a mass ratio of 7:3 as the solvent for the spinning solution; PVDF-HFP was selected, and the PVDF-HFP nanofiber membrane with ideal radiation cooling function was synthesized by electrospinning technology. The specific method is as follows: The PVDF-HFP particles were dissolved into the mixed solution with a mass concentration of 20%, magnetically stirred overnight until fully dissolved, and the spinning solution was obtained. The electrospinning process parameters were adjusted to make the spinning liquid eject stably, and an infusion pump was used to extract the spinning liquid collected in the syringe through the needle at a speed of 0.5 ml $hour^{-1}$. The distance between the setting pin and the grounded receiving plate is 10 cm, and a high voltage DC voltage of 20 kV is applied. After the spinning solution spraying was completed, a large-area PVDF-HFP radiation cooling film was successfully prepared.

Fabrication of thermoelectric arrays

SWCNTs aqueous dispersion (32 g) and waterborne polyurethane (8 g) were added into a mixed solution with a mass ratio of 8:2 and stirred magnetically at 25°C for 3 hours to obtain a uniformly mixed CNT mixed solution with a mass fraction of 0.16 wt %. The above CNT mixed solution was concentrated in an oven at 70°C for 12 hours to obtain a CNT slurry with a mass fraction of 0.64 wt %. The CNT slurry was added to a screen mold with 28 thermoelectric arrays and printed on the fabric at room temperature. The fabric was dried in an oven at 60°C for 1.5 hours. Then, the silver paste was added with 28 arrays of screen molds and printed on the above drying fabric at room temperature. The CNT thermoelectric module can be obtained by drying the above fabric in an oven at 60°C for 1.5 hours.

Fabrication of solar TEG

The PVDF-HFP nanofiber membranes were directly spun on the thermoelectric arrays to prepare a solar TEG.

Optical characterization of samples

The spectroscopic performance of samples was characterized separately in the ultraviolet (UV) to near-infrared (0.25 to 2.5 μm) and mid-infrared (2.5 to 20 μm) wavelength ranges. In the first range, the optical reflectance spectrum was measured using a UV-visible–near-infrared spectrophotometer (PE950, Shimadzu) equipped with an integrating sphere model (the diffuse standard pellets are polytetrafluoroethylene) pellets. For the second range, a Fourier transform infrared spectrometer (Nicolet IS50, Thermo Fisher Scientific) and a gold integrating sphere were used to measure the absorption spectra.

Microscopy measurement

The morphologies images of the radiative cooling samples were characterized by a scanning electron microscope (Regulus 8100, Hitachi).

Refractive index measurement

Refractive index measurements of PVDF-HFP matrix prepared by spin-coating method were taken by an IR-VASE ellipsometer (J. A. Woollam, USA).

Supplementary Materials

This PDF file includes:

Supplementary Text
Figs. S1 to S22
Tables S1 and S2

REFERENCES AND NOTES

1. M. Waqar, H. Wu, K. P. Ong, H. Liu, C. Li, P. Yang, W. Zang, W. H. Liew, C. Diao, S. Xi, D. J. Singh, Q. He, K. Yao, S. J. Pennycook, J. Wang, Origin of giant electric-field-induced strain in faulted alkali niobate films. *Nat. Commun.* **13**, 3922 (2022).
2. G. Du, J. Wang, Y. Liu, J. Yuan, T. Liu, C. Cai, B. Luo, S. Zhu, Z. Wei, S. Wang, S. Nie, Fabrication of advanced cellulosic triboelectric materials via dielectric modulation. *Adv. Sci.* **10**, e2206243 (2023).
3. B. Jiang, W. Wang, S. Liu, Y. Wang, C. Wang, Y. Chen, L. Xie, M. Huang, J. He, High figure-of-merit and power generation in high-entropy GeTe-based thermoelectrics. *Science* **377**, 208–213 (2022).
4. L. Li, S. Feng, Y. Bai, X. Yang, M. Liu, M. Hao, S. Wang, Y. Wu, F. Sun, Z. Liu, T. Zhang, Enhancing hydrovoltaic power generation through heat conduction effects. *Nat. Commun.* **13**, 1043 (2022).
5. P. Luo, Y.-M. Cao, B.-B. Han, Y.-B. Xue, Y.-D. Zhao, B. Wu, X.-X. Dong, C. Wang, W. Li, B.-B. Li, Y.-M. Xie, Y.-L. Xu, Z.-S. Wang, M. Zheng, M.-P. Zhuo, Nanosheets array-induced nanofluidic channels toward efficient primary batteries-coordinated textiles. *Nano Energy* **118**, 108988 (2023).
6. Y. B. Xue, Y. M. Cao, P. Luo, X. X. Dong, B. B. Han, Y. D. Zhao, M. Zheng, M. Zheng, Z. S. WangM, P. J. Zhuo, Asymmetric sandwich Janus structure for high-performance textile-based thermo–hydroelectric generators toward human health monitoring. *Adv. Funct. Mater.* **34**, 2310485 (2024).
7. H. C. Ates, P. Q. Nguyen, L. Gonzalez-Macia, E. Morales-Narváez, F. Güder, J. J. Collins, C. Dincer, End-to-end design of wearable sensors. *Nat. Rev. Mater* **7**, 887–907 (2022).
8. S. Guan, J. Li, Y. Wang, Y. Yang, X. Zhu, D. Ye, R. Chen, Q. Liao, Multifunctional MOF-derived Au, co-doped porous carbon electrode for wearable sweat energy harvesting-storage hybrid system. *Adv. Mater.* **35**, e2304465 (2023).
9. Q. Yang, S. Yang, P. Qiu, L. Peng, T.-R. Wei, Z. Zhang, X. Shi, L. Chen, Flexible thermoelectrics based on ductile semiconductors. *Science* **377**, 854–858 (2022).
10. L. Yin, F. Yang, X. Bao, W. Xue, Z. Du, X. Wang, J. Cheng, H. Ji, J. Sui, X. Liu, Y. Wang, F. Cao, J. Mao, M. Li, Z. Ren, Q. Zhang, Low-temperature sintering of Ag nanoparticles for high-performance thermoelectric module design. *Nat. Energy* **8**, 665–674 (2023).
11. K. Hu, D. Yang, Y. Hui, H. Zhang, R. Song, Y. Liu, J. Wang, P. Wen, D. He, X. Liu, Y. Yan, X. Tang, Optimized thermal design for excellent wearable thermoelectric generator. *J. Mater. Chem. A* **10**, 24985–24994 (2022).
12. J.-W. Li, Z. Han, J. Yu, H.-L. Zhuang, H. Hu, B. Su, H. Li, Y. Jiang, L. Chen, W. Liu, Q. Zheng, J.-F. Li, Wide-temperature-range thermoelectric n-type Mg_3 (Sb, Bi) $_2$ with high average and peak *zT* values. *Nat. Commun.* **14**, 7428 (2023).
13. W. B. Han, S.-Y. Heo, D. Kim, S. M. Yang, G.-J. Ko, G. J. Lee, D.-J. Kim, K. Rajaram, J. H. Lee, J.-W. Shin, T.-M. Jang, S. Han, H. Kang, J. H. Lim, D. H. Kim, S. H. Kim, Y. M. Song, S.-W. Hwang, Zebra-inspired stretchable, biodegradable radiation modulator for all-day sustainable energy harvesters. *Sci. Adv.* **9**, eadf5883 (2023).
14. C. Hou, M. Zhu, Semiconductors flex thermoelectric power. *Science* **377**, 815–816 (2022).
15. Y. Jia, Q. Jiang, H. Sun, P. Liu, D. Hu, Y. Pei, W. Liu, X. Crispin, S. Fabiano, Y. Ma, Y. Cao, Wearable thermoelectric materials and devices for self-powered electronic systems. *Adv. Mater.* **33**, 2102990 (2021).
16. L. Zhu, L. Tian, S. Jiang, L. Han, Y. Liang, Q. Li, S. Chen, Advances in photothermal regulation strategies: From efficient solar heating to daytime passive cooling. *Chem. Soc. Rev.* **52**, 7389–7460 (2023).
17. H. Wang, Q. Dong, J. Yao, Z. Shao, J. Ma, X. Chen, Colorless silk/copper sulfide hybrid fiber and fabric with spontaneous heating property under sunlight. *Biomacromolecules* **21**, 1596–1603 (2020).
18. S. Zeng, S. Pian, M. Su, Z. Wang, M. Wu, X. Liu, M. Chen, Y. Xiang, J. Wu, M. Zhang, M. Zhang, Q. Cen, Y. Tang, X. Zhou, Z. Huang, R. Wang, A. Tunuhe, X. Sun, Z. Xia, M. Tian, M. Chen, X. Ma, L. Yang, J. Zhou, H. Zhou, Q. Yang, X. Li, Y. Ma, G. Tao, Hierarchical-morphology metafabric for scalable passive daytime radiative cooling. *Science* **373**, 692–696 (2021).
19. J. Chang, L. Shi, M. Zhang, R. Li, Y. Shi, X. Yu, K. Pang, L. Qu, P. Wang, J. Yuan, Tailor-made white photothermal fabrics: A bridge between pragmatism and aesthetic. *Adv. Mater.* **35**, e2209215 (2023).
20. X. Zhao, T. Li, H. Xie, H. Liu, L. Wang, Y. Qu, S. C. Li, S. Liu, A. H. Brozena, Z. Yu, J. Srebric, L. Hu, A solution-processed radiative cooling glass. *Science* **382**, 684–691 (2023).
21. N. Kim, S. Lienemann, I. Petsagkourakis, D. Alemu Mengistie, S. Kee, T. Ederth, V. Gueskine, P. Leclère, R. Lazzaroni, X. Crispin, K. Tybrandt, Elastic conducting polymer composites in thermoelectric modules. *Nat. Commun.* **11**, 1424 (2020).
22. Y. An, Y. Fu, J.-G. Dai, X. Yin, D. Lei, Switchable radiative cooling technologies for smart thermal management. *Cell Rep. Phys. Sci.* **3**, 101098 (2022).
23. M.-D. Li, X.-Q. Shen, X. Chen, J.-M. Gan, F. Wang, J. Li, X.-L. Wang, Q.-D. Shen, Thermal management of chips by a device prototype using synergistic effects of 3-D heat-conductive network and electrocaloric refrigeration. *Nat. Commun.* **13**, 5849 (2022).
24. Y. D. Zhao, W. Jiang, S. Zhuo, B. Wu, P. Luo, W. Chen, M. Zheng, J. Hu, K.-Q. Zhang, Z.-S. Wang, L.-S. Liao, M.-P. Zhuo, Stretchable photothermal membrane of NIR-II charge-transfer cocrystal for wearable solar thermoelectric power generation. *Sci. Adv.* **9**, eadh8917 (2023).
25. C. Chen, B. Zhao, R. Wang, Z. He, J. L. Wang, M. Hu, X. L. Li, G. Pei, J. W. Liu, S.-H. Yu, Janus Helical ribbon structure of ordered nanowire films for flexible solar thermoelectric devices. *Adv. Mater.* **34**, 2206364 (2022).
26. Z. Wang, Y. Bo, P. Bai, S. Zhang, G. Li, X. Wan, Y. Liu, R. Ma, Y. Chen, Self-sustaining personal all-day thermoregulatory clothing using only sunlight. *Science* **382**, 1291–1296 (2023).
27. X. Zhang, Y. Hou, Y. Yang, Z. Wang, X. Liang, Q. He, Y. Xu, X. Sun, H. Ma, J. Liang, Y. Liu, W. Wu, H. Yu, H. Guo, R. Xiong, Stamp-like energy harvester and programmable information encrypted display based on fully printable thermoelectric devices. *Adv. Mater.* **35**, 2207723 (2023).
28. W. Ren, Y. Sun, D. Zhao, A. Aili, S. Zhang, C. Shi, J. Zhang, H. Geng, J. Zhang, L. Zhang, J. Xiao, R. Yang, High-performance wearable thermoelectric generator with self-healing, recycling, and Lego-like reconfiguring capabilities. *Sci. Adv.* **7**, eabe0586 (2021).
29. M. Yang, W. Zou, J. Guo, Z. Qian, H. Luo, S. Yang, N. Zhao, L. Pattelli, J. Xu, D. S. Wiersmainterfaces, Bioinspired "skin" with cooperative thermo-optical effect for daytime radiative cooling. *ACS Appl. Mater. Interfaces* **12**, 25286–25293 (2020).
30. T. Sun, B. Zhou, Q. Zheng, L. Wang, W. Jiang, G. J. Snyder, Stretchable fabric generates electric power from woven thermoelectric fibers. *Nat. Commun.* **11**, 572 (2020).
31. R. Lu, A. Shokrieh, C. Li, B. Zhang, K. Amin, L. Mao, Z. Wei, PVDF-HFP layer with high porosity and polarity for high-performance lithium metal anodes in both ether and carbonate electrolytes. *Nano Energy* **95**, 107009 (2022).
32. A. Babu, I. Aazem, R. Walden, S. Bairagi, D. M. Mulvihill, S. J. Pillai, Electrospun nanofiber based TENGs for wearable electronics and self-powered sensing. *Chem. Eng. J.* **452**, 139060 (2023).
33. B. Zhu, W. Li, Q. Zhang, D. Li, X. Liu, Y. Wang, N. Xu, Z. Wu, J. Li, X. Li, P. B. Catrysse, W. Xu, S. Fan, J. Zhu, Subambient daytime radiative cooling textile based on nanoprocessed silk. *Nat. Nanotechnol.* **16**, 1342–1348 (2021).
34. L. Xiong, Y. Wei, C. Chen, X. Chen, Q. Fu, H. Deng, Thin lamellar films with enhanced mechanical properties for durable radiative cooling. *Nat. Commun.* **14**, 6129 (2023).
35. X. Wang, M. Zhu, X. Li, Z. Qin, G. Lu, J. ZhaoZ, J. Zhang, Ultralow-power and radiation-tolerant complementary metal-oxide-semiconductor electronics utilizing enhancement-mode carbon nanotube transistors on paper substrates. *Adv. Mater.* **34**, 2204066 (2022).
36. Y. He, X. Lin, Y. Feng, B. Luo, M. Liu, Carbon nanotube ink dispersed by chitin nanocrystals for thermoelectric converter for self-powering multifunctional wearable electronics. *Adv. Sci.* **9**, 2204675 (2022).
37. W. Zhou, Q. Fan, Q. Zhang, L. Cai, K. Li, X. Gu, F. Yang, N. Zhang, Y. Wang, H. Liu, W. Zhou, S. Xie, High-performance and compact-designed flexible thermoelectric modules enabled by a reticulate carbon nanotube architecture. *Nat. Commun.* **8**, 14886 (2017).
38. Z.-H. Zheng, X.-L. Shi, D.-W. Ao, W.-D. Liu, M. Li, L.-Z. Kou, Y.-X. Chen, F. Li, M. Wei, G.-X. Liang, P. Fan, G. Q. (Max) Lu, Z.-G. Chen, Harvesting waste heat with flexible Bi_2Te_3 thermoelectric thin film. *Nat. Sustain.* **6**, 180–191 (2023).
39. Q.-X. Hu, W.-D. Liu, L. Zhang, W. Sun, H. Gao, X.-L. Shi, Y.-L. Yang, Q. Liu, Z.-G. Chen, SWCNTs/Ag_2Se film with superior bending resistance and enhanced thermoelectric performance via *in situ* compositing. *Chem. Eng. J.* **457**, 141024 (2023).
40. Y. Jing, J. Luo, X. Han, J. Yang, Q. Liu, Y. Zheng, X. Chen, F. Huang, J. Chen, Q. Zhuang, Correction: Scalable manufacturing of a durable, tailorable, and recyclable multifunctional woven thermoelectric textile system. *Energ. Environ. Sci.* **16**, 4693–4693 (2023).

Acknowledgments

Funding: We appreciate the financial support of National Natural Science Foundation of China (52203234) "Textile Vision Basic Research Program" (J202310), Key Laboratory of Silk Functional Materials and Technology, Key Laboratory of Flame Retardancy Finishing of Textile Materials, and Priority Academic Program Development of Jiangsu Higher Education Institutions (PAPD).
Author contributions: Conceptualization: J.-Z.L., W.J., and M.-P.Z. Methodology: M.-P.Z. and K.-Q.Z. Investigation: J.-Z.L., W.J., and M.-P.Z. Visualization: S.Z., Y.R., and Y.-Y.L. Supervision: H.L.,

J.H., W.C., and X.-Q.W. Writing—original draft: J.-Z.L., M.-P.Z., and K.-Q.Z. Writing—review and editing: J.-Z.L., M.-P.Z., and L.-S.L. **Competing interests:** The authors declare that they have no competing interests. **Data and materials availability:** All data needed to evaluate the conclusions in the paper are present in the paper and/or the Supplementary Materials.

Submitted 24 June 2024
Accepted 27 November 2024
Published 3 January 2025
10.1126/sciadv.adr2158